

Strong photoluminescence and high piezoelectric properties of Eu-doped $(\text{Ba}_{0.99}\text{Ca}_{0.01})(\text{Ti}_{0.98}\text{Zr}_{0.02})\text{O}_3$ ceramics

Zhe Wang¹ · Wei Li¹ · Ruiqing Chu² · Jigong Hao¹ · Zhijun Xu² · Guorong Li³

Received: 28 June 2017 / Accepted: 17 July 2017 / Published online: 24 July 2017
© Springer Science+Business Media, LLC 2017

Abstract Lead-free luminescent multifunctional $(\text{Ba}_{0.99}\text{Ca}_{0.01})_{1-x}\text{Eu}_x(\text{Ti}_{0.98}\text{Zr}_{0.02})\text{O}_3$ ($x=0, 0.002, 0.004$ and 0.006) (BCEZT- x) ceramics were successfully synthesized using solid state reaction method. The effects of Eu addition on the phase structure and electrical properties of the BCEZT- x ceramics were systematically studied. Results show that orthorhombic–tetragonal (O–T) phase transitions temperature decreases with increasing Eu content, and coexistence of the O and T phases is observed near room temperature (RT) in the composition range of 0.002–0.004. All the BCEZT- x ceramics exhibit high Curie temperature ($T_C > 115$ °C), especially $T_C \approx 120$ °C for the composition of $x=0.002$. The BCEZT- x ceramics at $x=0.002$ exhibit excellent piezoelectric properties ($d_{33}=400$ pC/N and $k_p = 52\%$), due to the coexistence of the O and T phase at RT. Meanwhile, a large strain S_{\max} of $\sim 0.22\%$ is obtained at $x=0.004$ for the BCEZT- x ceramics. Moreover, studies on photoluminescence properties of the ceramics shows that luminescence properties are strongly dependent on the doping concentration for the BCEZT- x ceramics. The strongest photoluminescence occurs at $x=0.004$ of the BCEZT- x ceramics. Upon the excitation of 465 nm

light, all the BCEZT- x ceramics have two intense emission peaks around 593 nm and 616 nm. According to the CIE chromaticity diagram, the ceramics possess a bright yellow light ($x=0.483, y=0.4991$). These results indicate that the BCEZT- x ceramics have significant technological potential as multifunctional devices due to their excellent electric and luminescence properties.

1 Introduction

Nowadays, lead-based perovskite piezoceramics have been widely used as universal actuators, sensors and transducers in the electromechanical fields, due to their superior piezoelectric properties near the morphotropic phase boundary (MPB) between rhombohedral and tetragonal phases [1, 2]. In spite of their outstanding properties, the impact of Pb element containing in ceramics on the environment has caused extensive concern of researchers. With the improvement of environmental awareness, some new groups of lead-free piezoelectric ceramics have been researched as alternative of commercial Pb-contained materials mostly. These groups include $(\text{K}_{0.5}\text{Na}_{0.5})\text{NbO}_3$ (KNN-based), $(\text{Bi}_{0.5}\text{Na}_{0.5})\text{TiO}_3$ (BNT-based) and BaTiO_3 (BT-based) piezoceramics [3–8]. Among them, the BT-based ceramics are considered as one of the most promising candidates for replacing lead-based piezoelectric ceramics because of the excellent electrical properties ($d_{33} \geq 300$ pC/N). In recent years, the researches of BT-based $(\text{Ba}, \text{Ca})(\text{Ti}, \text{Zr})\text{O}_3$ systems and $(\text{Ba}, \text{Ca})(\text{Ti}, \text{Sn})\text{O}_3$ systems have drawn many researchers' attentions [9, 10], due to their improved piezoelectric properties near polymorphic phase transitions (PPT) between the tetragonal and orthorhombic (T–O) phases or the coexistence of rhombohedral and orthorhombic phases [11] at RT, because the phase coexistence at

✉ Wei Li
liweili_727@163.com

Zhijun Xu
zhjxu@sohu.com

¹ College of Materials Science and Engineering, Liaocheng University, Liaocheng 252059, China

² School of Environmental and Materials Engineering, Yantai University, Yantai 264005, China

³ The State Key Lab of High Performance Ceramics and Superfinemicrostructure, Shanghai Institute of Ceramics, Chinese Academy of Science, Shanghai 200050, China

PPT can cause an easy polarization rotation of the dipole by an electric field or external stress [12–14].

With the intensive development of micro electro mechanical systems (MEMS), integration and digitization, multifunctional materials possessing two or more desirable properties in a single entity have attracted numerous interest in recent years, owing to their excellent coupling of piezoelectric, magnetic, dielectric, semiconducting and luminescence properties. Various two-parameter coupling effects, such as magneto-optical coupling [15], ferroelectric-elastic coupling [16], have been considerably observed and extensively studied by the scientific community. It is well known that rare earth elements are often used to obtain excellent photoluminescence (PL) materials as activator ions, by doping in piezoelectric perovskite ceramics. Zhang et al. [17] have fabricated Er^{3+} -doped BaTiO_3 ceramics and investigated the temperature dependence of PL spectra. Jia et al. [18] and Hao et al. [19] have reported that the PL performance of the rare earth elements doped piezoelectric materials can be enhanced by the piezoelectric polarization. Zhang et al. [20] have prepared the Eu^{3+} -doped KNN materials and researched the relation between emission intensity and KNN, EuNbO_4 phases. Peng et al. [21] have investigated the excitation and emission spectra of Pr^{3+} doped $\text{CaBi}_2\text{Ta}_2\text{O}_9$ based bismuth layered-structure oxides. It is reasonable that doping rare earth elements provides an effective way to obtain high-performance multifunctional piezoelectric materials in practical application.

In this work, a new lead-free photoluminescence and piezoelectric material with the piezoelectric-photoluminescence coupling effect was fabricated by doping Eu element as the activator into $(\text{Ba}, \text{Ca})(\text{Ti}, \text{Zr})\text{O}_3$ (BCZT) ceramics. The PPT of BCZT were designed near the RT, owing to high its' piezoelectric response at RT. The $(\text{Ba}_{0.99}\text{Ca}_{0.01})_{1-x}\text{Eu}_x(\text{Ti}_{0.98}\text{Zr}_{0.02})\text{O}_3$ (BCEZT- x , $x=0-0.006$) ceramics were expected to exhibit both good piezoelectric properties and photoluminescence properties. The phase transitional behavior, photoluminescence, and electrical properties of BCEZT were systematically studied. Results show that Eu doped BCZT ceramics exhibit a strong 616 nm emission under the 465 nm light excitation while maintaining good piezoelectric properties. The results are expected to provide a guideline for searching the new multifunctional lead-free materials in practical application.

2 Materials and methods

The $(\text{Ba}_{0.99}\text{Ca}_{0.01})_{1-x}\text{Eu}_x(\text{Ti}_{0.98}\text{Zr}_{0.02})\text{O}_3$ ($x=0, 0.002, 0.004$ and 0.006) lead-free ceramics, were synthesized by conventional solid state reaction method, using reagent-grade metal oxides or carbonate powders of CaCO_3 (Alfa Aesar,

99%), BaCO_3 (Alfa Aesar, 99%), TiO_2 (Alfa Aesar, 99.5%), ZrO_2 (Alfa Aesar, 99%) and Eu_2O_3 (Alfa Aesar, 99.99%) as starting materials. The raw materials were weighed at stoichiometric proportion and then mixed homogeneously by planetary ball milling in a polyethylene with stabilized zirconia balls for 12 h, using anhydrous ethanol as liquid medium. After drying, the mixed powders were calcined at 1250°C for 4 h in air. After calcination, the mixture was milled again for 12 h. The powders were mixed with an appropriate amount of Polyvinyl Alcohol (PVA), and then pressed into pallets with a diameter of 12 mm and thickness of 1.0 mm under the pressure of 200 MPa. The pallets mixed with PVA were burning off the binder at 750°C for 6 h for evaporating all the binder. After burning off the binder, the ceramics were sintered in an alumina crucible at 1450°C for 4 h in air.

The ceramic crystallization behavior was examined with an X-ray diffraction (XRD) meter with a $\text{Cu K}\alpha$ radiation ($\lambda=1.54178\text{ \AA}$) (D8 Advance, Bruker Inc., Karlsruhe, Germany). For the electrical properties, silver electrodes were coated on the top and bottom surfaces of the ceramics for the subsequent electrical measurements. Impedances spectroscopy of the samples was performed using a Broadband dielectric spectrometer (Novocontrol Germany) in the 0.01–20 MHz frequency range at various temperatures. The piezoelectric constant d_{33} was measured by a tester quasi-static d_{33} meter (YE2730 SINOCERA, Yangzhou, China). The electric field-induced polarization (P–E) and strain (S–E) were measured at RT at 10 Hz by using an aix-ACCT TF2000FE-HV ferroelectric test unit (aix ACCT Systems GmbH, Aachen, Germany). The temperature dependence of dielectric properties were measured by a capacitance meter (Agilent 4294 A, Agilent Inc., American) at temperatures ranging from 20°C to 180°C with a heating rate of $3^\circ\text{C}/\text{min}$. Luminescence properties was measured by a 465 nm laser using a spectrophotofluorometer (FLS920, Edinburgh, UK).

3 Results and discussion

Figure 1a shows the XRD patterns of the BCEZT- x ceramics at the 2θ range of $20^\circ-70^\circ$. A pure perovskite structure is obtained with no secondary or impure phases being detected, indicating that Eu^{3+} ions have diffused into BCZT lattices to form a homogeneous solid solution BCEZT- x within the studied doping level. Close inspection of the XRD patterns at the 2θ range of $43.5^\circ-46.5^\circ$ and $65^\circ-67^\circ$ are shown in Fig. 1b and c, respectively. The orthorhombic symmetry of the BCEZT- x ceramics at RT is characterized by an obvious peak of (200) at around 2θ of 45.5° for the composition $x<0.002$. With increasing Eu content, the BCEZT- x ceramics ($0.002\leq x\leq 0.004$) begin to

Fig. 1 The XRD patterns of the BCEZT-*x* ceramics at the 2θ range: (a) 20° – 70° , (b) 43.5° – 46.5° and (c) 65° – 67°

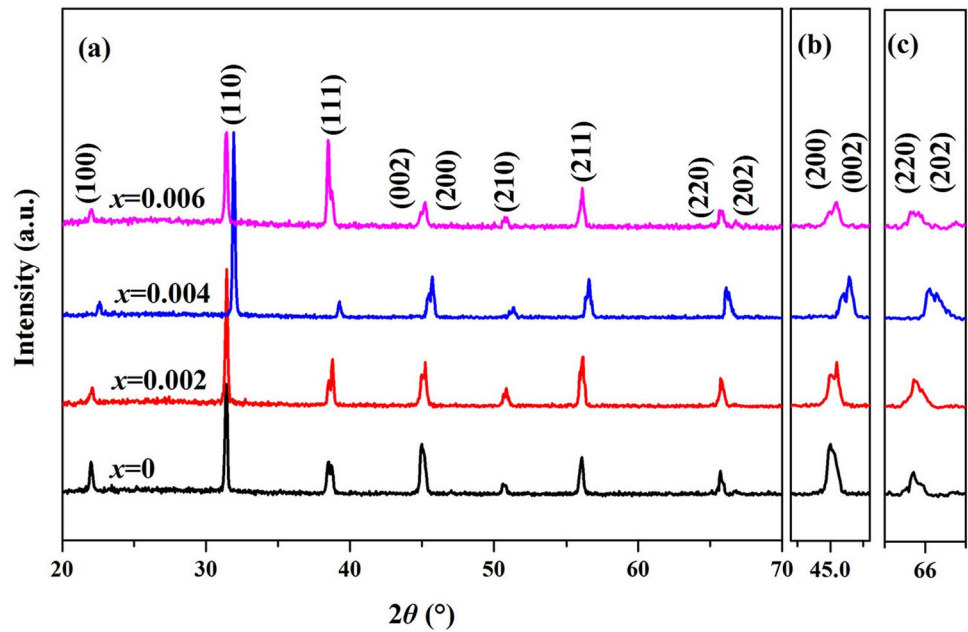


exhibit tetragonal symmetry, which is featured with splitting of (200)/(002) peaks at around 2θ of 45° and (220)/(202) peaks at 2θ of 65.5° [22, 23]. The obvious splitting of the (200)/(002) peaks at around 2θ of 45° indicates that the BCEZT-*x* ceramics possess pure tetragonal symmetry at

$x \geq 0.006$ [24]. Therefore, it can be suggested that the phase transition from orthorhombic phase to tetragonal phase shifts with increasing Eu content and the BCEZT-*x* ceramics at the compositions of 0.002–0.004 exhibit the coexistence of tetragonal and orthorhombic phases at RT.

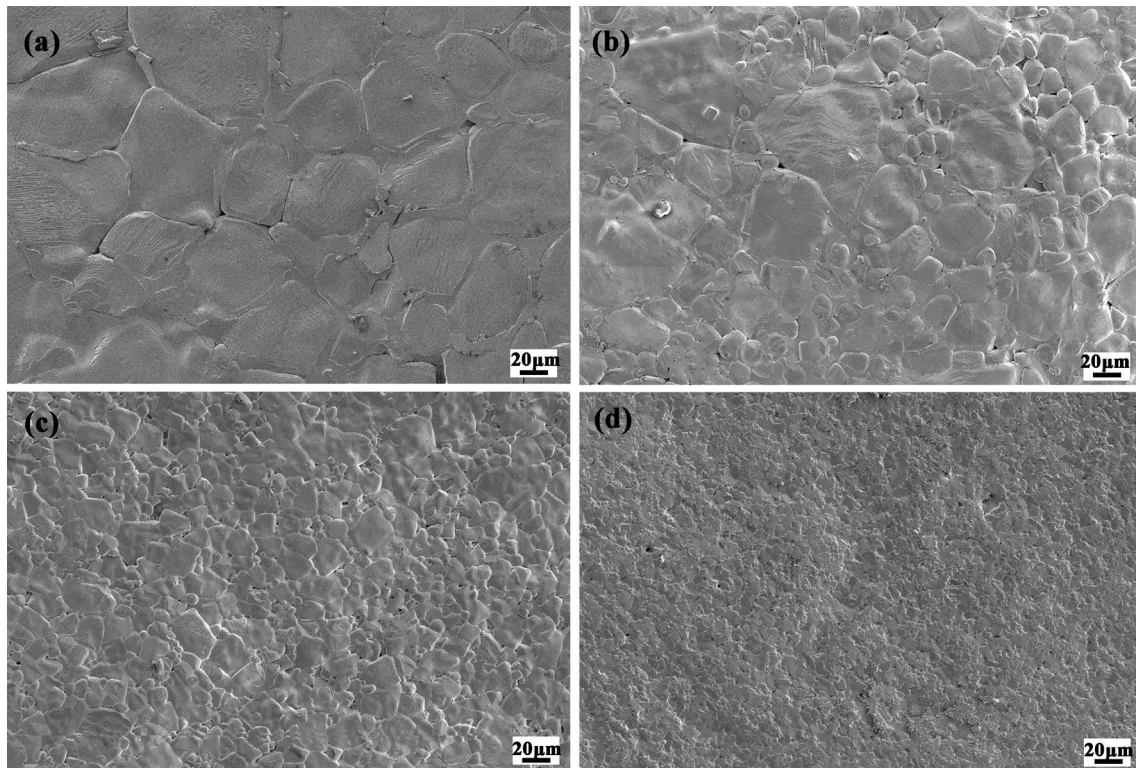


Fig. 2 The FE-SEM images of the BCEZT-*x* ceramics at **a** $x=0$, **b** $x=0.002$, **c** $x=0.004$ and **d** $x=0.006$

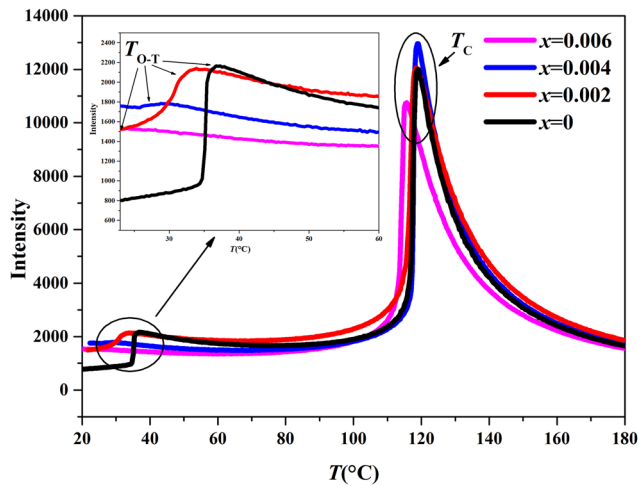


Fig. 3 The temperature dependence of dielectric constant ϵ_r of the BCEZT- x ceramics ($x=0, 0.002, 0.004$ and 0.006) measured at 100 kHz (the inset is the dielectric constant ϵ_r of BCEZT- x ceramics between 20 to 60 °C)

Figure 2 shows the SEM images of the BCEZT- x ceramics observed on the surface of the compositions at (a) $x=0$, (b) $x=0.002$ (c) $x=0.004$ and (d) $x=0.006$. The surface microstructure of the BCEZT- x ceramics appears homogeneous and few pores exist in the grain boundary. The relative density of BCEZT- x ceramics sintered at 1450 °C reach up to highest value of 96%, indicating that all the BCEZT- x ceramics are well sintered. As shown in Fig. 2a–d, addition of Eu causes a significant change in grain size. The grain size decreases gradually with increasing Eu content. It is suggested that addition of rare earth ions in BCZT ceramics can inhibit the grain growth because of their relatively low diffusivity [25]. This result is similar to that observed in other lead-free piezoceramics like Eu-doped KNN ceramics [26] and Eu-doped BFO-BT ceramics [27].

Figure 3 illustrates temperature dependence of the relative permittivity constant (ϵ_r) of the BCEZT- x ceramics at $x=0, 0.002, 0.004$ and 0.006 measured at frequency of 100 kHz between 20 and 180 °C. The two pronounced ϵ_r peaks at the compositions of $x=0-0.004$ are corresponded to the two phase transitions: O–T phase transition at the temperature (T_{O-T}) $\approx 20-35$ °C and tetragonal–cubic (T–C) phase transition at the temperature (T_C) $\approx 115-120$ °C [9]. For the composition of $x=0.006$, the T_{O-T} disappears in this figure, indicating that the T_{O-T} of the BCEZT- x ceramics at $x=0.006$ is lower than RT. The O–T phase transitions show a significant change with the compositions. As shown in the inset of the Fig. 3, the O–T phase transitions of the BCEZT- x ceramics gradually shifts toward lower temperature with increasing Eu³⁺ content. The decrease of T_{O-T} and broad region of O–T phase transition maybe due to the unit cell shrinkage effect with the substitutions of smaller Eu³⁺

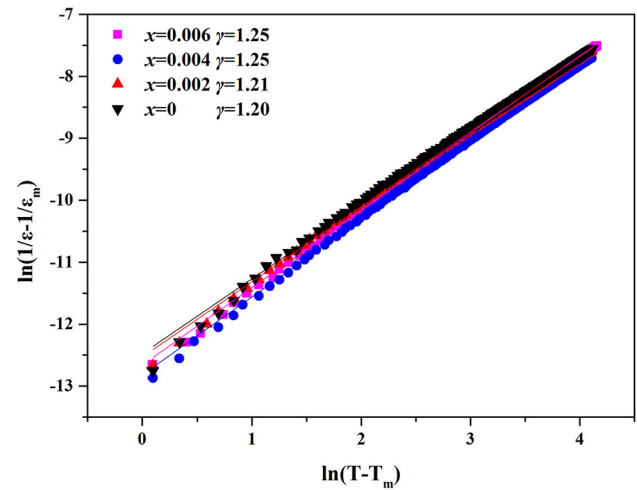


Fig. 4 Plot of $\ln(1/\epsilon_r - 1/\epsilon_m)$ as a function of $\ln(T - T_m)$ for the BCEZT- x ($x=0, 0.002, 0.004$ and 0.006) ceramics at 10 kHz

(1.23 Å) [28] for Ba²⁺ (1.35 Å) in this work [29]. The T_C for each ceramic is above 115 °C, especially $T_C \approx 120$ °C for the composition of $x=0.002$. These results indicate that the usage temperature range of the BCEZT- x ceramics could be essentially broadened, which is important in exploiting the piezoceramics from the application point of view [15].

To illuminate the matter of the phase transition, the degree of diffusion (γ) was calculated by a modified empirical expression [30] of Curie–Weiss law to describe the phase transition character of the BCEZT- x ceramics:

$$\frac{1}{\epsilon} - \frac{1}{\epsilon_m} = \frac{1}{C}(T - T_m)^\gamma \quad (1)$$

where ϵ is the dielectric constant, ϵ_m is the dielectric constant maximum, T is the temperature ($>T_C$), T_m is the temperature at the dielectric peak, γ is the relaxation strength and C is the Curie constant [31]. The value of γ is between 1 and 2, giving the information on the phase transition diffuseness degree of ferroelectrics: $\gamma=1$ for normal ferroelectric related to a sharp phase transition, $\gamma=2$ for ideal relaxor ferroelectric and $1 \leq \gamma \leq 2$ denote a diffuse phase transition [29]. Figure 4 shows the logarithmic plot of this empirical expression. The slopes of the logarithmic plot are the values of γ for the BCEZT- x ceramics. The γ value increases gradually from 1.20 to 1.25 with increasing Eu content, illustrating that the relaxor ferroelectric increases in the BCEZT- x ceramics. In other words, increasing Eu substitution promotes the phase transition more diffuse in the BCEZT- x ceramics.

Figure 5a–d shows complex impedance spectra of the BCEZT- x ceramics from 0.01 Hz to 20 MHz and from 300 to 425 °C. Two semicircles can be observed clearly,

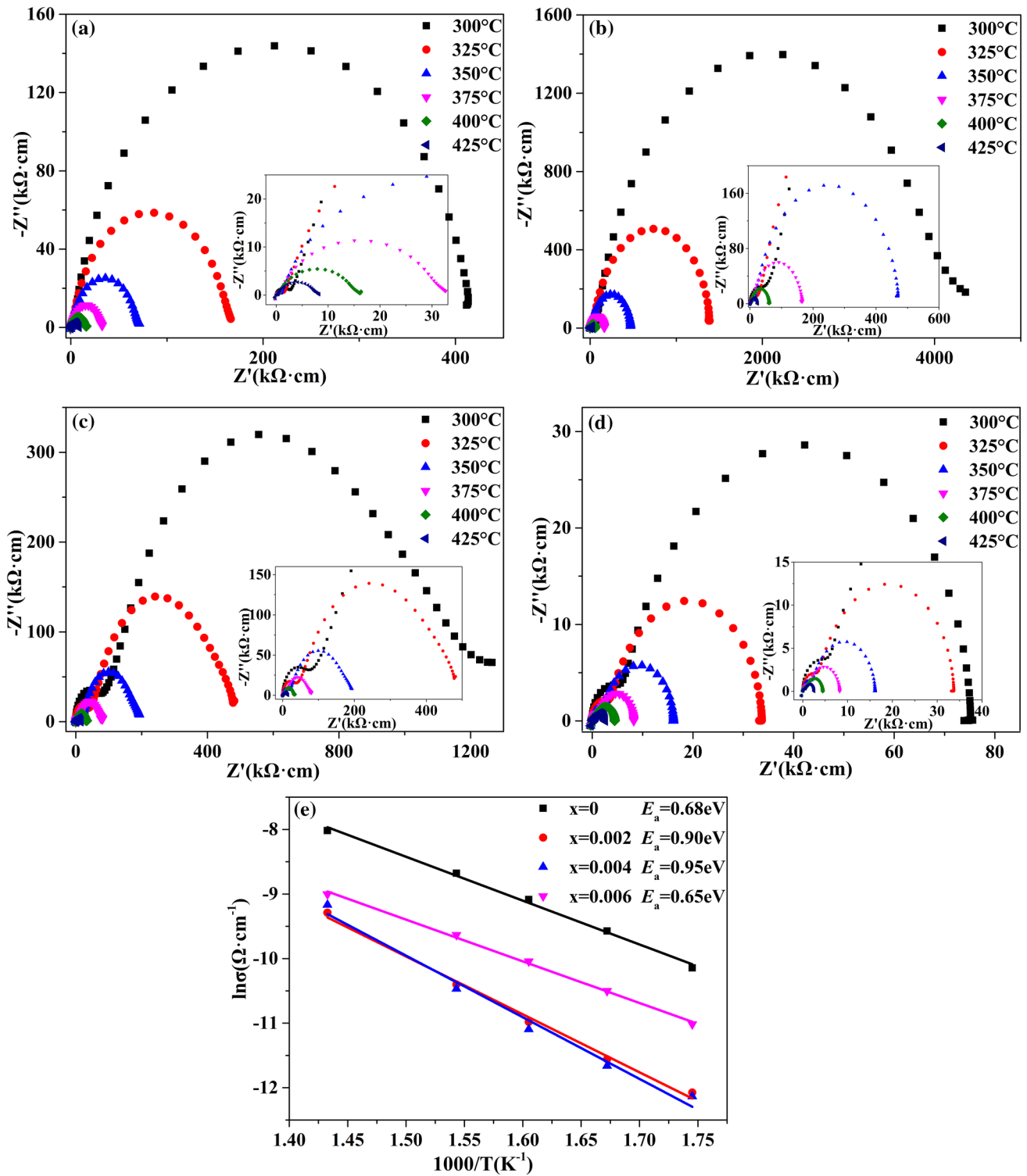


Fig. 5 The impedance spectra of the BCEZT-*x* **a** $x=0$, **b** $x=0.002$, **c** $x=0.004$ and **d** $x=0.006$ ceramics in the frequency range of 0.01 Hz to 20 MHz between 300 and 425 °C and **e** Arrhenius plots of σ dc conductivity of the BCEZT-*x* ceramics

attributing to the grain and grain-boundary conductivities, respectively [4]. The small semicircles at high frequency reflect the properties of grain, while the large semicircles

at lower frequency range correspond to the behavior of ceramic grain boundary [32]. With increasing the heating temperature, the semicircles gradually contract, which

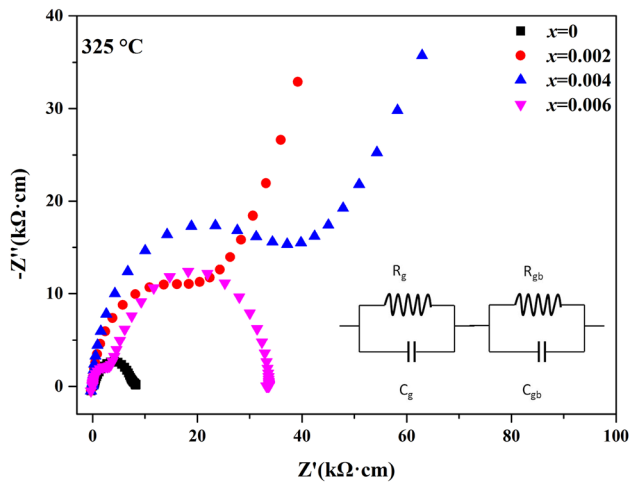


Fig. 6 The impedance spectra of the BCEZT- x ceramics ($x=0, 0.002, 0.004$ and 0.006) at $325\text{ }^{\circ}\text{C}$; the inset shows an equivalent circuit for the BCEZT- x ceramics

results in the increase of conductivity (σ) [33]. In addition, the relation between activation energy (E_a) and σ can be denoted by the Arrhenius law:

$$\sigma = \sigma_0 \exp(-E_a/kT) \quad (2)$$

where σ_0 is a constant, k is the Boltzmann constant and T is the absolute temperature. The logarithms of conductivity σ vs. reciprocal temperature $1000/T$ of the BCEZT- x ceramics are shown in Fig. 5e. The best least-squares fitting of Eq. (2) are marked by the solid lines. The corresponding activation energies E_a of BCEZT- x ceramics are calculated to be 0.68, 0.90, 0.95, and 0.65 eV, respectively. It has been reported that the value of E_a for A- and B-site cations in ABO_3 perovskite materials were 4 and 12 eV, respectively [34]. For oxygen vacancies, it varies from 0.5 to 2 eV approximately, depending on their concentration [35]. Therefore, it is reasonable to suggest that oxygen vacancies dominate the conductivity of the BCEZT- x ceramics in the temperature range of $300\text{--}425\text{ }^{\circ}\text{C}$ [36]. Figure 6 shows

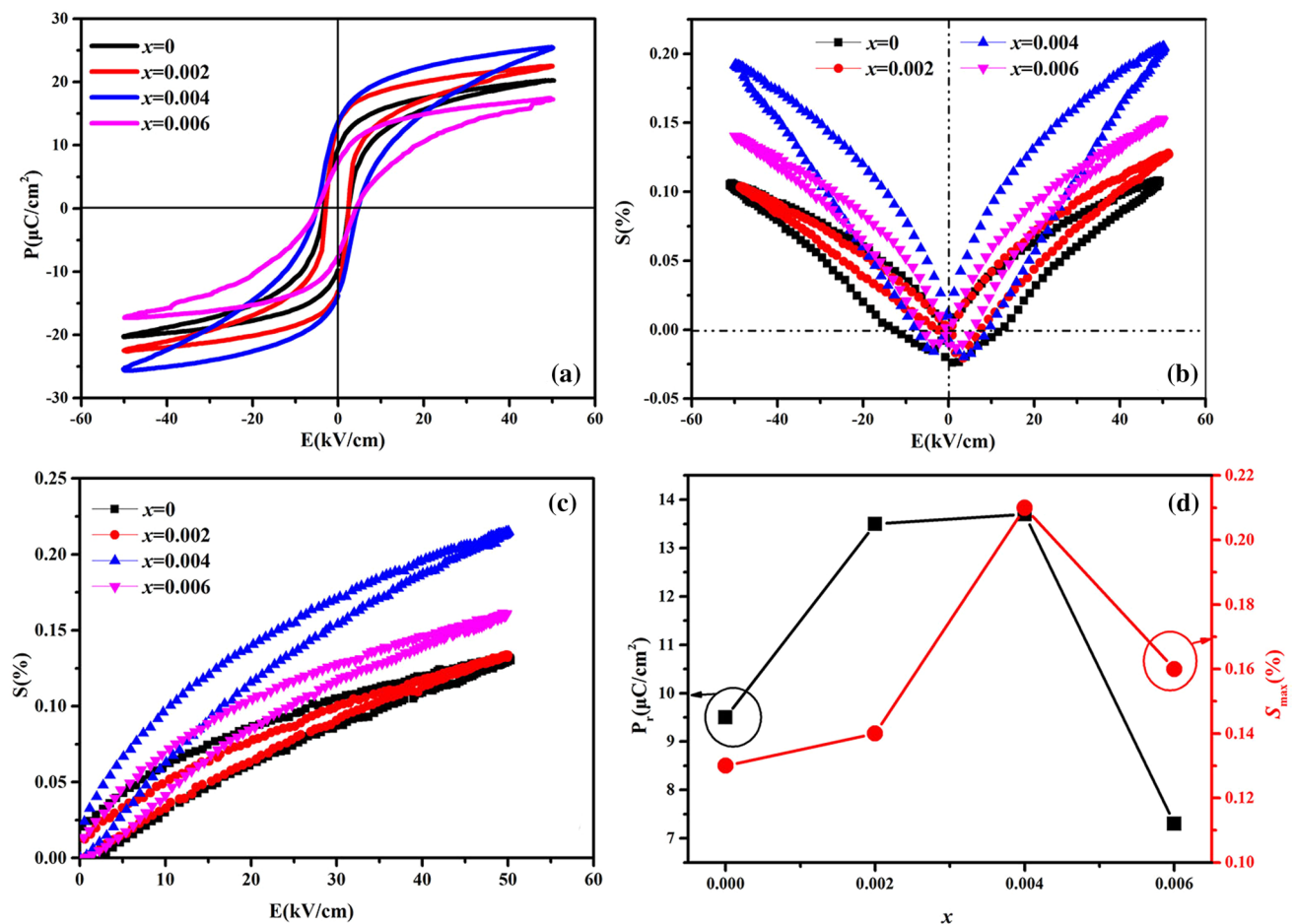


Fig. 7 **a** The P - E hysteresis loops, **b** bipolar field-induced strain curves, **c** unipolar field-induced strain curves and **d** remnant polarization (P_r) and strain (S_{\max}) as functions of x of the BCEZT- x ceramics measured at RT and a frequency of 10 Hz

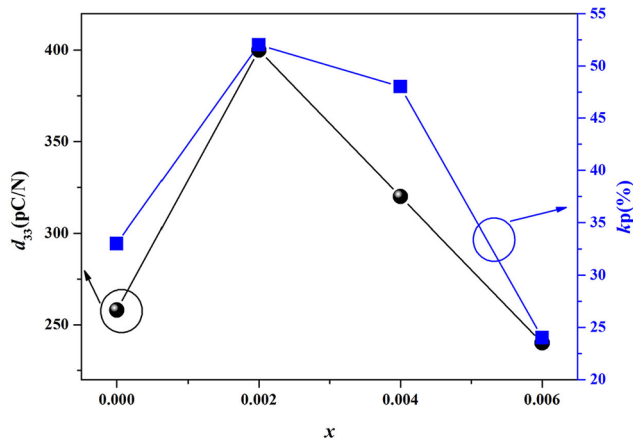


Fig. 8 Piezoelectric coefficient (d_{33}) and planar mode electromechanical coupling coefficient (k_p) of the BCEZT- x ceramics measured at RT

complex impedance spectra of the BCEZT- x ceramics with different Eu^{3+} elements. With increasing of Eu^{3+} elements, the resistivity firstly increases and then decreases. The equivalent circuit for the BCEZT- x ceramics is shown in the inset of Fig. 6, first semicircle in impedance spectra can be represented by parallel combination of resistance (R_g) and capacitance (C_g) of grains whereas second semicircle is the combination of R_{gb} and C_{gb} of grains. For all ceramics, the values of R_{gb} are considerably larger than R_g , indicating the better insulating performance of the grain boundaries [37].

The ferroelectric hysteresis (P - E) loops, bipolar field-induced strain (S - E) curves, unipolar field-induced strain curves and remnant polarization (P_r) and Strain (S_{max}) as functions of x of the BCEZT- x ceramics are shown in Fig. 7, respectively. All of the measurements were carried out at RT and 10 Hz. It is clear that all the BCEZT- x ceramics exhibit a typical P - E loop with relatively large remnant polarization (P_r) and low coercive field (E_c) (<5 kV/cm). With increasing Eu content, the value of P_r increases significantly with x until it reaches the highest value of $13.7 \mu\text{C}/\text{cm}^2$ at $x=0.004$, before decreasing to $7.3 \mu\text{C}/\text{cm}^2$ at $x=0.006$. The largest values of P_r are obtained at the compositions of $x=0.002$ - 0.004 with the coexistence of O-T polymorphic phase transition, owing to the facilitated polarization switching to the orthorhombic spontaneous polarization directions or tetragonal polarization directions during the poling treatment [38, 39]. As shown in Fig. 7b, all the ceramics exhibit an analogous butterfly-shaped curve. The enhancement effect in the strain properties is more obvious, and a large strain about 0.21% of the BCEZT- x ceramics is obtained at $x=0.004$. Figure 7c shows the unipolar S - E curves of the BCEZT- x ceramics. The change of unipolar S - E curves with x is similar to that

of P - E loops and S - E curves. The P_r and S_{max} as functions of x of the BCEZT- x ceramics are shown in Fig. 7d, respectively.

The dependences of piezoelectric constant (d_{33}) and planar mode electromechanical coupling coefficient (k_p) with x for the BCEZT- x ceramics are shown in Fig. 8. The observed d_{33} and k_p values increase significantly with increasing x until they reach the highest value of $d_{33}=400$ pC/N and $k_p=52\%$ at $x=0.002$, and then decreases gradually with further increase of Eu content. The significant enhancement in piezoelectric properties of the BCEZT- x ceramics at 0.002-0.004 should be attributed to the high P_r , low E_c , and multiphase coexistence at RT, as shown in P - E loops and ϵ_r - T curves. Better piezoelectric properties obtained by a large remnant polarization and the poling process of the ceramics facilitated by a low coercive field [40]. Meanwhile, near the PPT region, the number of the possible spontaneous polarization direction of the ceramics increases and thus the ceramics can be poled easily. The compositions of $x < 0.002$ and $x > 0.004$ are at orthorhombic phase and tetragonal phase, respectively. Therefore, the piezoelectric properties of these compositions are inferior to that of the compositions of $x=0.002$ - 0.004 .

Figure 9a illustrates the PL and PL emission (PLE) spectra of the BCEZT- x ceramics. The PL spectra of the ceramics were measured by monitoring the emission at 614 nm, exhibiting an intense and sharp absorption peak centered at 465 nm. The peak is ascribed to the $4f-5d$ (${}^7F_0-{}^5D_2$) electronic transitions [41]. The PLE spectra of the ceramics upon excitation at 465 nm are also provided. Excited at 465 nm, a strong yellow emission occurs in a single phase of the BCEZT- x ceramics. Figure 9b shows the energy level diagram of Eu^{3+} ions, which clearly illustrates the photoluminescence process. According to the energy level diagram of Eu^{3+} and selection rules, when electrons are excited to 5D_2 levels, the 5D_2 levels radiationlessly relax to the 5D_0 and 5D_1 states, and subsequently recombine to 7F_J ($J=1-4$) levels. The emission peaks of Eu^{3+} centered at 550, 593, 616, 653 and 699 nm correspond to ${}^5D_1-{}^7F_1$, ${}^5D_0-{}^7F_1$, ${}^5D_0-{}^7F_2$, ${}^5D_0-{}^7F_3$ and ${}^5D_0-{}^7F_4$ transitions. Figure 9c illustrates the dependence of the Eu content on the emission intensity of the ${}^5D_0-{}^7F_2$ transitions centered at 616 nm of the BCEZT- x ceramics. The emission intensity of the ${}^5D_0-{}^7F_2$ transitions increases gradually with x until it reaches the highest value at $x=0.004$. Beyond the critical concentration of $x=0.004$, a decrease in the emission intensity is clearly observed, illustrating that energy migration occurs between Eu^{3+} ions in BCZT lattice, then resulting in concentration quenching. This is in accordance with the report by Zhang et al. [42]. The calculated CIE chromaticity diagram of BCEZT-0.004 ceramics excited by 465 nm is shown in Fig. 9d. It is believed that the BCEZT- x ceramics

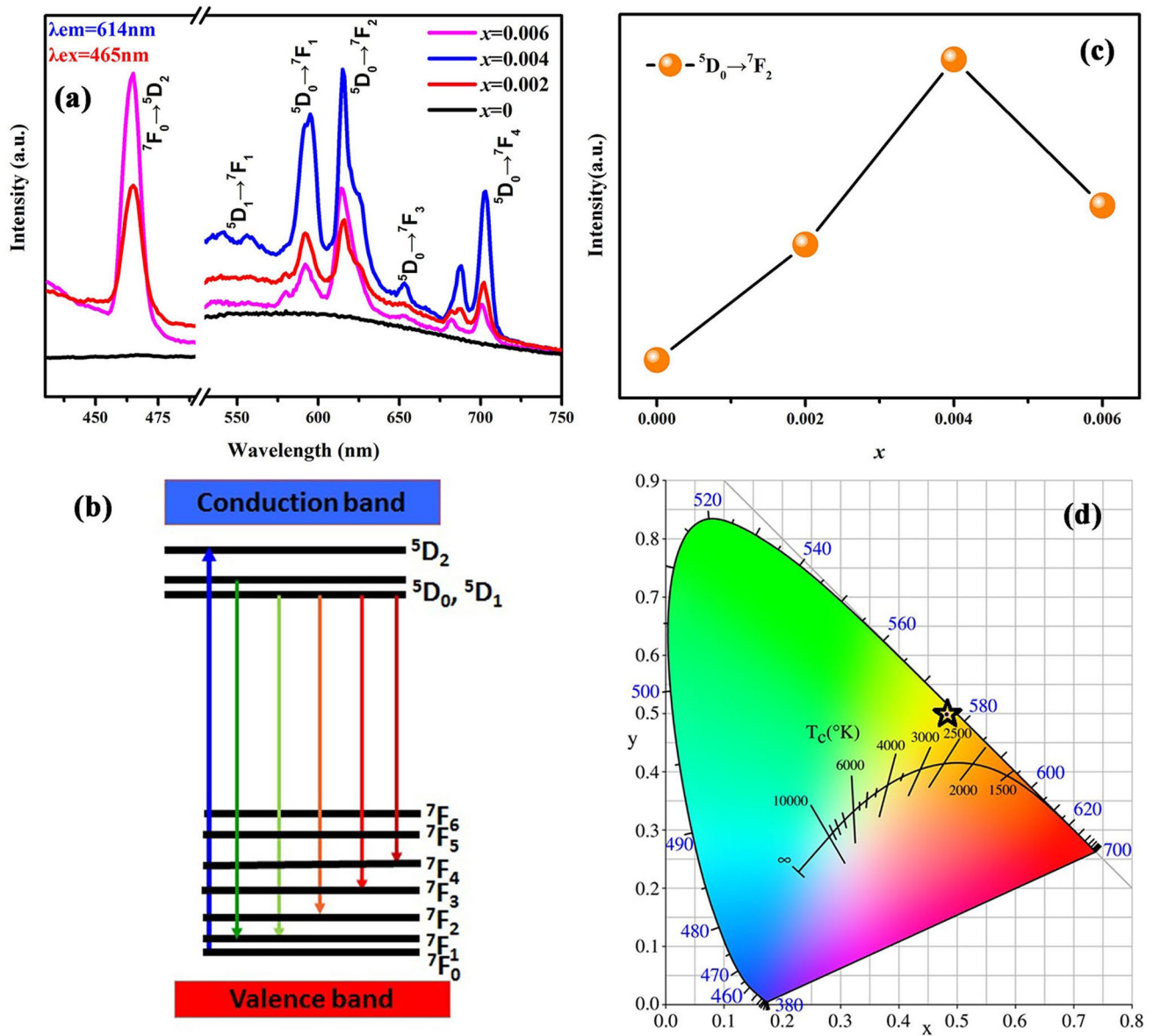


Fig. 9 **a** The PL and PLE spectra of the BCEZT- x ($x=0.002, 0.004$ and 0.006) ceramics ($\lambda_{em}=614$ nm, $\lambda_{ex}=465$ nm) at RT, **b** energy level diagram of the Eu^{3+} ions, **c** the emission intensity of the $5D_0$ -

$7F_2$ transitions centered at 616 nm and **d** CIE chromaticity diagram excited by 465 nm

exhibit yellow-emitting properties according to the point ($x=0.483, y=0.4991$) in the figure.

4 Conclusions

The BCEZT- x ($x=0, 0.002, 0.004$ and 0.006) ceramics were successfully synthesized by solid state reaction method. The phase structure and electrical properties of the BCEZT- x ceramics were systematically investigated. The PPT from orthorhombic phase to tetragonal phase is observed at RT in the composition range of 0.002–0.004.

All the BCEZT- x ceramics exhibit high Curie temperature of ($T_C > 115$ °C). The BCEZT- x ceramics exhibit good piezoelectric properties ($d_{33}=400$ pC/N and $k_p = 52\%$) at $x=0.002$ and large strain S_{max} of $\sim 0.22\%$ at $x=0.004$, due to the coexistence of tetragonal phase and orthorhombic phase at RT. Moreover, excellent luminescence properties are obtained under the excitation of 465 nm at RT for BCEZT- x ceramics, particularly at $x=0.004$. All the BCEZT- x ceramics have two intense emission peaks around 593 and 616 nm, respectively. According to the CIE chromaticity diagram, the ceramics possess a bright yellow light ($x=0.483, y=0.4991$). These results suggest that the

BCEZT-*x* ceramics with high piezoelectric properties and strong luminescence properties have potential applicability as multifunctional materials.

Acknowledgements This work was supported by the National Key R&D Program of China (No. 2016YFB0402701), the National Natural Science Foundation of China (No. 51372110, 51402144 and 51502127), the Natural Science Foundation of Shandong Province of China (No. ZR2016EMM02 and ZR2014JL030) and the Project of Shandong Province Higher Educational Science and Technology Program (No. J14LA11 and J14LA10).

References

- L.F. Zhu, B.P. Zhang, L. Zhao, S. Li, Y. Zhou, X.C. Shi, N. Wang, *J. Eur. Ceram. Soc.* **36**, 1017–1024 (2016)
- Q.R. Lin, D.Y. Wang, S. Li, *J. Am. Ceram. Soc.* **98**, 2094–2098 (2015)
- X.Q. Huo, R. Zhang, L.M. Zheng, S.J. Zhang, R. Wang, J.J. Wang, S.J. Sang, B. Yang, W.W. Cao, *J. Am. Ceram. Soc.* **98**, 1829–1835 (2015)
- P.Q. Long, X.T. Liu, X. Long, Z.G. Yi, *J. Alloys Compd.* **706**, 234–243 (2017)
- S.H. Shin, J.D. Han, J. Yoo, *Mater. Lett.* **154**, 120–123 (2015)
- Q. Zhang, B.P. Zhang, P. Zhao, H.T. Li, L.M. Zhang, *Rare Metals* **28**, 142–146 (2009)
- J. Tao, Z.G. Yi, Y. Liu, M.X. Zhang, J.W. Zhai, *J. Am. Ceram. Soc.* **96**, 1847–1851 (2013)
- W.F. Bai, D.Q. Chen, P. Zheng, J.H. Xi, Y. Zhou, B. Shen, J.W. Zhai, Z.G. Ji, *J. Eur. Ceram. Soc.* **37**, 2591–2604 (2017)
- J.G. Wu, D.Q. Xiao, W.J. Wu, Q. Chen, J.G. Zhu, Z.C. Yang, *J. Wang, Scr. Mater.* **65**, 771–774 (2011)
- W. Li, Z.J. Xu, R.Q. Chu, P. Fu, G.Z. Zang, *J. Am. Ceram. Soc.* **94**, 4131–4133 (2011)
- N.A. Spaldin, M. Fiebig, *Science* **309**, 391–392 (2005)
- L. Zhang, M. Zhang, L. Wang, C. Zhou, Z. Zhang, Y. Yao, L. Zhang, D. Xue, X. Lou, X. Ren, *Appl. Phys. Lett.* **105**, 162908 (2014)
- C. Zhou, W.F. Liu, D.Z. Xue, X.B. Ren, H.X. Bao, J.H. Gao, L.X. Zhang, *Appl. Phys. Lett.* **100**, 222910 (2012)
- W. Li, Z.J. Xu, R.Q. Chu, Z.H. Wu, J.G. Hao, P. Fu, J. Du, Z.X. Yue, *RSC Adv.* **5**, 91903–91907 (2015)
- J. Rodel, W. Jo, K.T.P. Seifert, E.M. Anton, T. Granzow, D. Damjanovic, *J. Am. Ceram. Soc.* **92**, 1153–1177 (2009)
- S.C. Hwang, C.S. Lynch, R.M. McMeeking, *Acta Metall. Mater.* **43**, 2073–2084 (1995)
- Y. Zhang, J.H. Hao, C.L. Mak, X.H. Wei, *Opt. Exp.* **19**, 1824–1829 (2011)
- X.L. Tian, Z. Wu, Y.M. Jia, J.R. Chen, R.K. Zheng, Y.H. Zhang, H.S. Luo, *Appl. Phys. Lett.* **102**, 042907 (2013)
- J.H. Hao, Y. Zhang, X.H. Wei, *Angew. Chem.* **123**, 7008–7012 (2011)
- H.Q. Sun, Q.W. Zhang, X.S. Wang, M. Gu, *Mater. Res. Bull.* **64**, 134–138 (2015)
- D.F. Peng, H.Q. Sun, X.S. Wang, J.C. Zhang, M.M. Tang, X. Yao, *J. Alloys Compd.* **511**, 159–162 (2012)
- P.Z. Zhang, M.R. Shen, L. Fang, F.G. Zheng, X.L. Wu, J.C. Shen, H.T. Chen, *Appl. Phys. Lett.* **92**, 222908 (2008)
- K.C. Singh, A.K. Nath, R. Laishram, O.P. Thakur, *J. Alloys Compd.* **509**, 2597–2601 (2011)
- W. Li, Z.J. Xu, R.Q. Chu, P. Fu, G.Z. Zang, *J. Am. Ceram. Soc.* **93**, 2942–2944 (2010)
- Q. Zhang, X.H. Zhu, Y.H. Xu, H.B. Gao, Y.J. Xiao, D.Y. Liang, J.L. Zhu, J.G. Zhu, D.Q. Xiao, *J. Alloys Compd.* **546**, 57–62 (2013)
- L.B. Fei, D.P. Shi, Y.M. Huang, L.J. Liu, *J. Mater. Sci.* **26**, 7159–7164 (2015)
- M.J. Tian, L. Zhou, X. Zou, Q.J. Zheng, L.L. Luo, N. Jiang, D.M. Lin, *J. Mater. Sci.* **26**, 8840–8847 (2015)
- L. Yu, J.G. Hao, Z.J. Xu, W. Li, R.Q. Chu, G.R. Li, *Ceram. Int.* **42**, 14849–14854 (2016)
- M.L. Chen, Z.J. Xu, R.Q. Chu, Z. Wang, S.S. Gao, G.H. Yu, W. Li, S.W. Gong, G.R. Li, *Mater. Res. Bull.* **59**, 305–310 (2014)
- K. Uchino, S. Nomura, *Ferroelectrics* **44**, 55–61 (1982)
- Z.R. Yao, R.Q. Chu, Z.J. Xu, J.G. Hao, J. Du, G.R. Li, *RSC Adv.* **6**, 13803–13808 (2016)
- J.Y. Miao, Z.Q. Zhang, Z.F. Liu, Y.X. Li, *Ceram. Int.* **41**, S487–S491 (2015)
- R.F. Cheng, Z.J. Xu, R.Q. Chu, J.G. Hao, J. Du, G.R. Li, *Ceram. Int.* **41**, 6424–6431 (2015)
- B.S. Kang, S.K. Choi, C.H. Park, *J. Appl. Phys.* **94**, 1904–1911 (2003)
- S. Steinsvik, R. Bugge, J. Gjønnes, J. Taftø, T. Norby, *J. Phys. Chem. Solids* **58**, 969–976 (1997)
- L. L. Li, J. G. Hao, Z. J. Xu, W. Li, R. Q. Chu, G. R. Li, *Ceram. Int.* **42**, 14886–14893 (2016)
- L. Zhang, H. Hao, H.X. Liu, Z. Song, Z.H. Yao, J. Xie, H.X. Liu, X.Y. Zhu, Q. Xu, X.C. Huang, M.H. Cao, *J. Eur. Ceram. Soc.* **36**, 3157–3163 (2016)
- D. Damjanovic, *J. Am. Ceram. Soc.* **88**, 2663–2676 (2005)
- M.L. Chen, Z.J. Xu, R.Q. Chu, H. Qiu, M. Li, Y. Liu, L. Shao, S. Ma, W.B. Ji, W. Li, S.W. Gong, G.R. Li, *Phys. B* **433**, 43–47 (2014)
- M.L. Liu, F.Y. Lei, N. Jiang, Q.J. Zheng, D.M. Lin, *Mater. Res. Bull.* **74**, 62–69 (2016)
- Y.M. Jia, Y.B. Wei, Z. Wu, Z.H. Zhou, J.R. Chen, Y.K. Jia, Y.H. Zhang, J.Y. Zhou, H.H. Wang, *J. Alloys Compd.* **586**, 66–68 (2014)
- Q.W. Zhang, H.Q. Sun, X.S. Wang, Y. Zhang, X. Li, *J. Eur. Ceram. Soc.* **34**, 1439–1444 (2014)